EO Polymer-Based Integrated-Optical Acoustic Spectrum Analyzer

Araz Yacoubian, Vadim Chuyanov, Sean M. Garner, William H. Steier, Albert S. Ren, and Larry R. Dalton

***Abstract*—An acoustic spectrum analyzer based on electrooptic (EO) polymer integrated optics is presented. The device is used in a scanning heterodyne geometry by zero biasing a Michelson interferometer. It is capable of detecting vibrations from DC to GHz range. The novelty of this work is applying EO polymers to high frequency acoustic sensing applications. EO polymers have been extensively used for communication devices. However, their use in high frequency sensing applications remains unexplored. The sensor presented here is designed to analyze thin film structure by utilizing high frequency capabilities of EO polymers. The advantage of this approach over existing methods is in its potential to detect vibrations over 100 GHz with low drive voltages (V_π less than 1 V), using a device that is completely electrically controlled with no mechanical moving parts. Low frequency tests indicate good agreement between experimental results and theoretical predictions. Acoustic vibrations excited by pulsed Nd-YAG laser are detected to frequencies up to 200 MHz using the device presented.**

***Index Terms*—Acoustic sensing, EO polymers, heterodyne detection, interferometric sensing.**

I. Introduction

HIGH-FREQUENCY acoustics is greatly important for analyzing fine structures and performing nondestructive evaluation (NDE) of materials opaque to electromagnetic radiation. An appropriate acoustic sensor should exhibit both the sensitivity and the frequency range required to provide fine spatial resolution. The highest sensitivity is generally achieved using optical interferometric systems [1]–[6]. When a passive interferometer is used for detecting vibration, the output is modulated at the vibration frequency. At high frequencies (GHz range), detectors and electronics are noisy and have low gain. For example, to analyze submicron structures using acoustic wavelength of 0.1 μm in a solid with sound velocity of 5 km/s, one needs to analyze 50 GHz vibrations. This frequency is out of the detection range of piezo transducers, and direct detection of the output of an interferometer requires photodetectors and electronics operating at frequencies greater than 50 GHz. Photodetector SNR is inversely proportional to bandwidth [7]. Therefore, downconversion allows detection of narrow band high frequency vibrations with low frequency detectors, resulting to higher SNR than one would obtain without heterodyning.

A device is proposed and analyzed that is capable of down converting gigahertz acoustic vibrations to kHz–MHz frequencies, making use of an electrooptic modulator. The downconverted signal is then detected using low frequency photodetectors and electronics. Therefore, detection of narrow band vibrations up to 50 GHz, for example, would require a RF signal source of up to 50 GHz, while requiring only a low frequency (kHz–MHz) photo-detector.

Recently, a technique called picosecond ultrasonics [8]–[22] has been used to analyze sub-micron structures and to analyze thin films. It utilizes a pump-probe geometry, and makes measurements in the time domain with the help of a moving mirror/prism used for optical delay. The sensor presented here is also designed to study thin films, but it senses acoustic waves in the frequency domain. It is highly sensitive because it is interferometric, and unlike picosecond ultrasonics, it does not have any mechanical moving parts. Instead it is completely electrically controlled, does not require vibration isolation since it is based on planar optical geometry, is compact and easily deployable [23]. Additionally, polymer-based sensors have the potential to be integrated with drive electronics [24]. The integrated optical device shown in Fig. 1 utilizes an electrooptic (EO) polymer as the active component of a heterodyning Michelson interferometer [25]–[27].

The use of polymer-based integrated optics has been well established for making high speed modulators for communication devices. However, their use for sensing applications remains relatively unexplored. To extend the frontiers of acoustic sensing, the same technology used in modulators operating over 100 GHz [28] and at sub-1-V drive voltages [29] is utilized here for acoustic spectrum analysis.

II. Device Concept and Theory of Operation

The schematic diagram of the device is shown in Fig. 1, which is a Michelson interferometer biased at zero phase difference between the two arms of the interferometer. Light is split into two via a directional coupler, one part is reflected from a mirrorized endface of the waveguide (reference), and the other is outcoupled and reflected back from the surface of the sample under test (signal). The reference and signal beams are combined at the photo-detector. The phase modulation on the light caused by the vibrating surface beats with the phase modulation due to

Manuscript received March 21, 2000; revised August 2, 2000.

A. Yacoubian was with the Department of Electrical Engineering–Electrophysics, University of Southern California, Los Angeles, CA 90089-0483. He is now with Integrated Photonic Technology (IPITEK) Corporation, Carlsbad, CA 92008 USA.

V. Chuyanov and W. H. Steier are with the Department of Electrical Engineering–Electrophysics, University of Southern California, Los Angeles, CA 90089-0483 USA.

S. M. Garner was with the Department of Electrical Engineering–Electrophysics, University of Southern California, Los Angeles, CA 90089-0483. He is now with Corning Inc., SPAR01, Corning, NY 14831 USA.

A. S. Ren and L. R. Dalton are with the Department of Chemistry, Loker Hydrocarbon Institute, University of Southern California, Los Angeles, CA 90089-1661 USA.

Publisher Item Identifier S 1077-260X(00)11240-7.

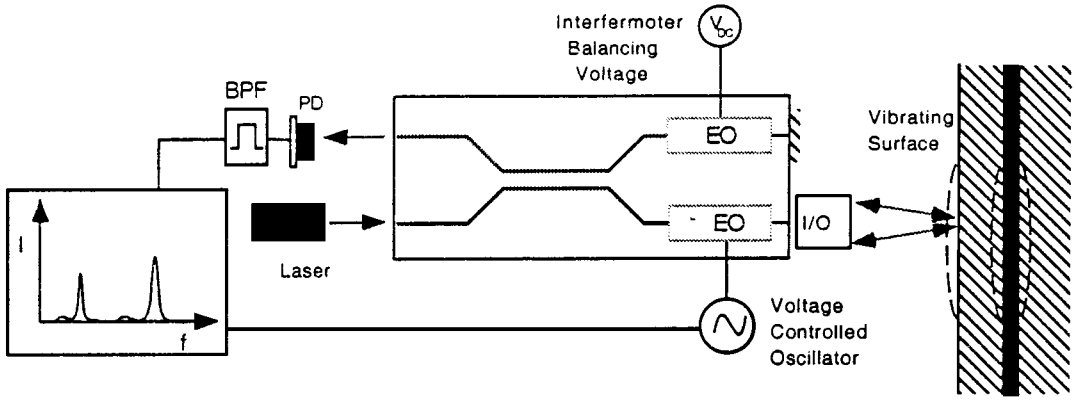

Fig. 1. Simplified schematic of a polymer-integrated optical acoustic spectrum analyzer. EO: electrooptic polymer phase modulator; I/O: input/output optics (GRIN lens or fiber coupled); BPF: bandpass filter. PD; photo-detector.

the EO polymer because the interferometer is biased at its maximum quadratic point. The vibration signal is downconverted to lower frequencies and is detected by a low frequency photodetector. Immediately after the detector, a low-pass (homodyne) or a bandpass (heterodyne) filter is utilized for filtering out the unwanted frequencies. When the beat frequency falls within the filter's bandwidth, a high signal is obtained, and when the beat frequency is out of the filter's range, a low signal is obtained. Thus, varying the EO modulation frequency yields a scan that corresponds to the acoustic spectrum of the vibrating surface.

The light intensity at the photodetector can be modeled as

$$I(t) = r(1-r)I_o \cdot \{2 + 2\cos[\phi_s \cos(\omega_s t) - \phi_m \cos(\omega_m t) + \phi_d]\} \quad (1)$$

where

- r coupling coefficient (0.5 for 50 : 50 coupler);
- ϕ_s $= (2\pi/\lambda)\Delta_s$;
- λ wavelength of light;
- Δ_s vibration amplitude;
- ϕ_m $= (2\pi/\lambda)\Delta n_{EO} L$;
- L modulator length;
- Δn_{EO} index variation due to electrooptic modulation;
- ϕ_d phase difference between the two arms of the interferometer.

The angular frequencies of vibration and EO modulation (denoted by subscripts s and m, respectively) are given by

$$\omega_{s,m} = 2\pi f_{s,m}. \quad (2)$$

Setting the interferometer to zero bias (i.e., $\phi_d = 0$), and for small amplitude vibrations (1) becomes

$$I(t) = r(1-r)I_o\{4 - [\phi_s^2 \cos^2(\omega_s t) + \phi_m^2 \cos^2(\omega_m t) - 2\phi_s\phi_m \cos(\omega_s t)\cos(\omega_m t)]\} \quad (3)$$

or

$$I(t) = r(1-r)I_o\left\{4 - \frac{\phi_s^2}{2} - \frac{\phi_m^2}{2} - \frac{\phi_s^2}{2} \cdot \cos(2\omega_s t) - \frac{\phi_m^2}{2}\cos(2\omega_m t) + \phi_s\phi_m \cos[(\omega_s - \omega_m)t] + \phi_s\phi_m \cdot \cos[(\omega_s + \omega_m)t]\right\}. \quad (4)$$

The most important is the difference $(\omega_s - \omega_m)$ term in the above equation, denoting frequency downconversion. Higher order terms are filtered by a low-pass or bandpass filter.

One of the advantages of using EO polymers is its ability to operate from as low as DC to over 100 GHz frequencies. To utilize this wide bandwidth characteristic of the polymers, the acoustic spectrum is obtained by scanning the EO modulation frequency and recording the signal that passes through the low-pass/bandpass filter. Alternatively, one would use a fixed EO modulation frequency, and instead use an electronic spectrum analyzer to observe the beat signal. However, this would limit the measurement capability, since *a priori* knowledge of the expected vibration frequency is necessary to carefully tune the EO modulation frequency.

To illustrate what one would expect from scanning the EO modulation frequency, simulations are carried out using (4), as shown in Fig. 2. Here, (a) a numerical low-pass and (b) a bandpass filtering scheme are implemented using FFT routine. In these simulations, the sample is assumed to vibrate at a specific frequency f_s, and the modulation frequency (f_m) is scanned. For simplicity, the plot is shown at normalized frequency axis. Here, 50 : 50 coupling was assumed ($r = 0.5$), and the vibration and modulation amplitudes were $\phi_s = \phi_m = 0.1$. The width of the observed signal was determined by the filter's upper frequency, which in this case was 0.2 at normalized frequency units. Relatively wide-band filters are used here to illustrate in detail what the observed signal would look like. In most of our experiments, much narrower bandwidth filters were used, resulting in narrower peaks in the acoustic spectra.

Although the signal using low-pass filter is generally higher than using a bandpass filter with the same upper frequency limit, heterodyning has a number of advantages. Near DC, detectors exhibit noise that has $1/f$ response [30], [31]. Thus, heterodyning removes the low frequency noise. Furthermore, heterodyning greatly reduces the noise due to the slow drift of the interferometer. One drawback of heterodyning is that it produces two peaks in the acoustic spectrum instead of one, located around the vibration frequency. This can limit the spectral resolution of the measurements. Therefore, filter selection is determined by the experimental conditions such as noise, acoustic amplitude, optical power received at the photo-detector, and by spectral resolution requirements.

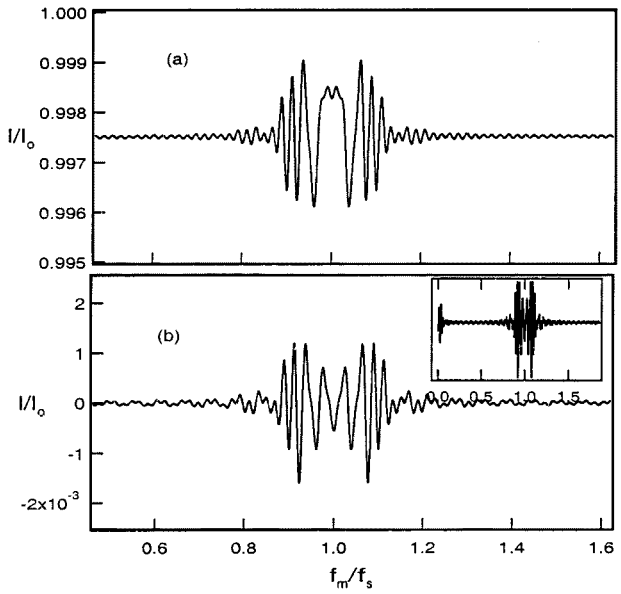

Fig. 2. Simulation of the acoustic spectrum analyzer using (a) low-pass and (b) bandpass filter configurations. A 50 : 50 coupler and $\phi_s = \phi_m = 0.1$ was assumed. Inset refers to complete spectral scan (to DC) used for amplitude calibration. The peak near DC occurs when $2f_m$ falls within the bandpass filter bandwidth.

The important parameters in acoustic spectrum analysis are the frequency of vibration, the amplitude, and the relative phase. The vibration frequency can be extracted from the spectrum by locating the center of the beat signal [e.g., the center lobe in Fig. 2(a)]. The beat signal is symmetrical around $f_m = f_s$ in the observed spectrum. At low amplitudes vibrations (much less than the optical wavelength, in this case 1.3 μm), the signal obtained from the scan is linearly proportional to the mirror vibration.

When a spectral scan is carried out to DC, a peak is observed at the lower frequency end of the spectrum [see inset of Fig. 2(b)]. This peak results from the $\cos(2\omega_m t)$ term in (4), when $2\omega_m$ falls within the bandpass filter bandwidth, and it can be used to obtain the vibration amplitude. When $\phi_m = 2\phi_s$, the observed spectrum will contain two peaks of the same height, one at the vibration frequency, and the second near DC. Therefore, knowledge of EO modulation amplitude ϕ_m, which is known from device parameters, yields the vibration amplitude. The relative phase difference between multiple vibrations can also be obtained from the shape of the recorded spectrum. The shape of the beat signal is dependent on the vibration phase, and observing shape differences between two vibration peaks yield information on their relative phase difference. For example, the central lobe of the signal shown in Fig. 2(b) is pointing downward. Delaying the vibration phase by π will result the central lobe to point upward. If one determines both the phase and the amplitude of vibrations, it is possible to obtain the time domain vibration signature by Fourier analysis, and thereby determine the subsurface structure of the sample under test [9], [32].

III. Experimental Results

The active material used in the device was a thermosetting chromophore/polymer system, FTC [33], which was thermally crosslinked during poling. The $r_{33} = 40$ pm/V at 1.06 μm, with layer thickness of 1.5–2 μm sandwiched between an upper and lower cladding. The lower cladding is 4 μm thermally curing epoxy (epoxilyte), and the upper cladding is 4-μm UV curable optical epoxy (norland 73). The waveguides are 7 μm wide and separated by 12 μm (center-to-center) in the directional coupler region, which is 7 mm long. They are patterned using UV lithography and reactive ion etched (RIE) to 0.15 μm ridge height. The final device length is 4 cm long.

The EO modulator electrodes were vacuum deposited (100 nm Au) and thickened to 3 μm by electroplating. Bulk electrode design was incorporated, with the cutoff frequency around 3–4 GHz.

The input/output of the device is provided by fiber pigtails or gradient index lenses, with the exception of the reference arm, where the endface of the waveguide is Au coated to provide back reflection. The optical source was a 1.3-μm diode laser.

The total insertion loss was 44 dB, mainly due to a propagation loss of 2–3 dB/cm, which resulted to 16–24 dB roundtrip loss for a 4-cm-long device and 3–6 dB loss per connection. The 2–3 dB/cm propagation loss is attributed mainly to material absorption due to C–H overtones and to scattering. Although this number is relatively high, a new generation of materials such as CLD-1/PMMA [29] have waveguide losses on the order of 1 dB/cm, which are being utilize for new generation of devices. Furthermore, alternative waveguide geometries are being investigated to drastically reduce the length and insertion loss of the device, such as utilizing diced grooves as beam splitters instead of using directional couplers [34].

A. Low Frequency Proof-of-Concept Experiments

Initial experiments were conducted using a low frequency piezo element with a thin reflective mirror pasted on it. The piezo element was set to vibrate at a certain frequency in the kHz range. The EO modulator was driven using a low frequency voltage-controlled oscillator. The frequency was scanned using a ramp voltage, and the signal from the photodetector was low-pass or bandpass filtered, amplified, and converted to digital signal using a 12-bit analog to digital (A/D) converter operating at 1 kHz. The result of a single scan is shown in Fig. 3 using both (a) low-pass and (b) bandpass filters. Each spectral scan time was 0.2 to 0.3 s, with 200–300 samples per scan. Soft edged analog low-pass (DC to 100 Hz) and bandpass (30 to 100 Hz) filters were used, which determined the spectral resolution of the scan. When a sharp-edged filter is used, the resolution of the acoustic spectrum is approximately equal to twice the upper frequency of the filter (care must be taken to use high enough A/D conversion rate to avoid undersampling). The analog filter used in these experiments resulted to spectral resolution of approximately 400 Hz. Results indicate the interferometer was operating as expected, as seen in the similarity between the simulated and experimental data shown in Figs. 2 and 3, respectively. To increase the SNR of detection, multiple consecutive scans were conducted and plotted on one graph.

To demonstrate the sensor as an acoustic spectrum analyzer capable of detecting multiple vibrations, two frequencies at 2.7 kHz (180 nm amplitude) and 4.0 kHz (330 nm amplitude) are applied to the piezo element. The results of ten consecutive

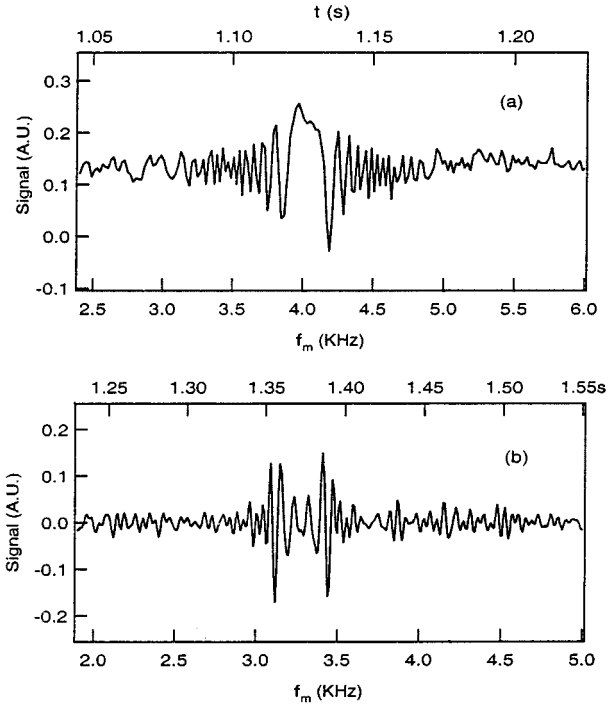

Fig. 3. Experimental signal output of the sensor indicating detection of vibration at 4 kHz using (a) low-pass filtering scheme (DC to 100 Hz) and (b) at 3.25 kHz using a bandpass filter (30 to 100 Hz). Vibration amplitude is 185 nm. Top axis refers to scan time.

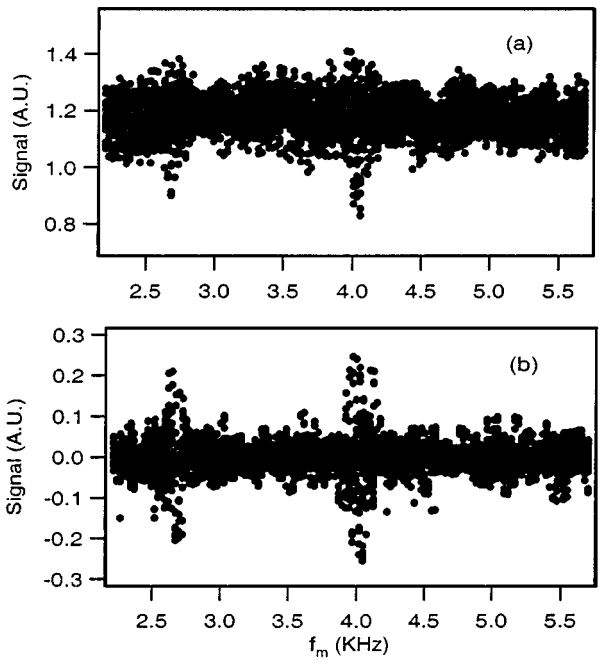

Fig. 4. (a) Signal after analog bandpass filtering, and (b) further digital bandpass filtered revealing both vibrations at 2.7 and 4 kHz (bandpass filter: 50–100 Hz).

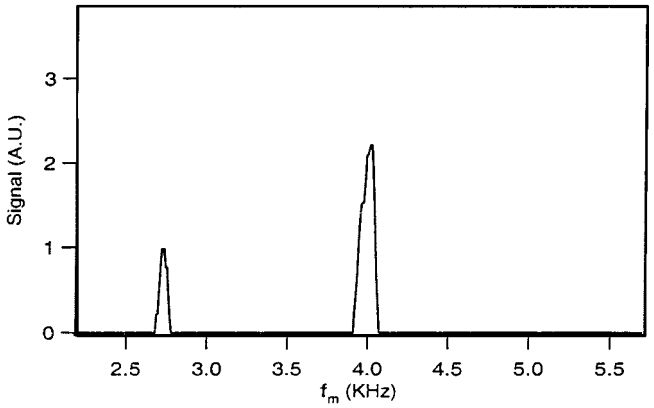

Fig. 5. Postprocessed data.

scans using an analog bandpass filter set between 50 and 100 Hz are shown in Fig. 4(a). Each scan duration was 0.34 s, with 423 sampling points resulting in a total of 3.4 s to complete ten spectral scans (4230 total samples). The purpose of conducting a fast scan was to avoid interferometer drift, because the sensor was not actively balanced.

The noise observed in the acoustic spectrum can be removed by postprocessing the data. In the experimental system, an analog bandpass filter is used after the photodetector. The filter can be tuned anywhere from DC to 100 kHz. However, it does not have sharp boundaries, making it difficult to filter out certain unwanted frequencies, such as the 60 Hz electric line noise. To overcome this problem, the data is further processed by utilizing digital filters (executed on a microcomputer).

One concern in an interferometric sensor is noise generated by mechanical vibrations and thermal fluctuations. Because the presented device has a planar geometry and both arms of the interferometer are at close proximity (300 μm apart) to each other, temperature fluctuations and mechanical vibrations induce approximately equal amount of phase changes to both arms of the interferometer and thus, the net effect is canceled. Signal fluctuations due to room temperature variations were negligible compared to mechanical vibrations, which were picked up by the input/output fiber. When a gradient index (GRIN) lens was used for I/O coupling, noise level was much lower than using a fiber I/O system. In our experiments, noise due to room vibrations were less than 50 Hz, which could be filter out by setting the low frequency limit of the bandpass filter higher than 50 Hz.

The data shown in Fig. 4(a) were digitally filtered using a rectangular filter with sharp upper and lower limits of 50 and 100 Hz. The resulting spectrum is shown in Fig. 4(b). Digital filtering resulted to 2–3 dB increase in the SNR. The spectra shown in Fig. 4 is the result of multiple scans. By summing all the scans, smoothing it with a moving average window, and thresholding, a clear spectrum is obtained as shown in Fig. 5. The resolution of the acoustic spectrum in these experiments was approximately 200 Hz.

B. Detection of a Pulsed-Laser Excited High Frequency Vibrations

To demonstrate the device at high frequencies and wide bandwidth, a 76 MHz mode-locked and Q-switched Nd-YAG laser is used to generate high frequency vibrations in an Si sample. The laser wavelength was 1.06 μm with a pulse width of 100 ps, and Q-switched at the rate of 1 kHz. The sample under test was a 2 $\times$ 2.5 cm, 410 μm thick [100] cut Si coated with 14.5 nm Cr. The experimental setup is shown in Fig. 6.

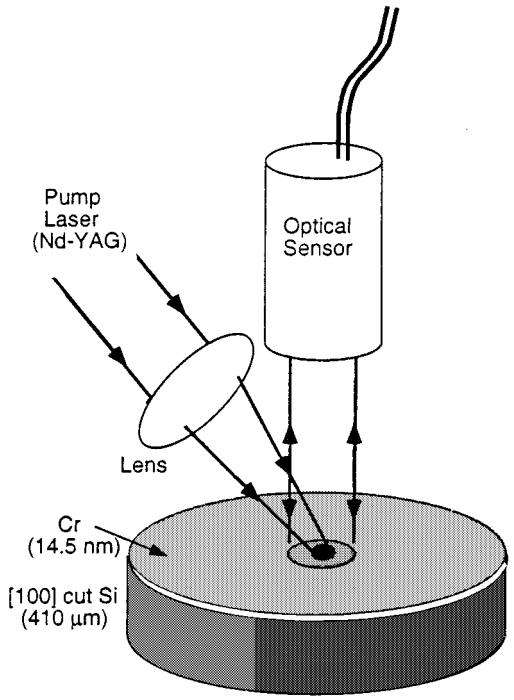

Fig. 6. Setup used for detecting pulse Nd-YAG laser excited vibrations.

The light from the Nd-YAG laser (pump) was focused on the sample with a spot size on the order of 10 μm. The 1.3 μm sensing arm of the interferometer (probe) was collimated via a GRIN lens attached to the end of a fiber, which was pigtailed to the device. The collimated beam had a 300 μm diameter. The angle between the pump and the probe beams was $\sim 25^{\circ}$. Both beams overlapped on the surface of the Si sample. The pump intensity was controlled by a variable attenuator.

The result of the heterodyne tests using seven consecutive frequency scans is shown in Fig. 7. A low frequency photodetector with a cutoff frequency at 300 kHz was used for detection. A programmable RF source was used, with an output power of 10 dBm (into a 50 Ω line) to drive the EO modulator on the device. The frequency was scanned from 1 MHz to 200 MHz. Frequency resolution of the spectrum was 600 kHz, determined by the cutoff frequency of the photodetector. Each frequency scan took 30 s to complete. Such a slow scan was due to the limiting speed of the computer program used for controlling the experiment and data acquisition. The interferometer was not actively balanced, thus, it went in and out of phase. Mixing occurs when the interferometer has quadratic response. Therefore, any deviation from zero phase difference will cause the signal (i.e., the beat between vibration and EO modulation) to decrease in amplitude. Therefore, it was necessary to conduct multiple frequency scans to ensure detection of all the vibration peaks. The 76 MHz peak is due to the mode-locked pulses. Other peaks were also observed at 31, 45, 100 MHz and higher. To understand the source of resonances, let us look at the sample structure. One possible explanation is standing waves caused by acoustic reflection from the front and back surfaces of the Si wafer. The sound velocity in Si is 8.2 km/s [13]. Therefore, the fundamental resonance is 10 MHz, and the third harmonic is 30 MHz. The material can also exhibit nonlinear elastic behavior,

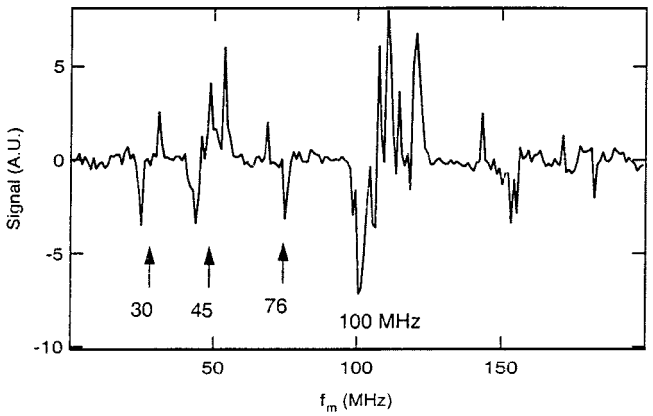

Fig. 7. Detection of pulsed laser-induced vibrations using the NLO polymer-based acoustic sensor.

which can give rise to sum and difference frequency generation [35], and the peaks observed at 45 and 100 could be due to this effect, namely, the beating of the 76 MHz and 30 MHz vibrations. The exact cause of these vibrations, however, cannot be determined with our experimental data, and more tests are needed, such as varying the intensity of the pump beam and observing the change in the spectrum.

The amplitudes of the peaks in Fig. 7 do not necessarily correspond to the exact acoustic amplitude, because the data are composed of different frequency scans, and during each scan the interferometer was susceptible to phase drift, which alters the amplitude of the detected resonances. Furthermore, the number of scans was not enough to result to a true average signal. The purpose of this experiment was to demonstrate the operation of the device to frequencies up to 200 MHz but not to give an accurate account of the sample vibration response. If the spectrum shown in Fig. 7 was calibrated for amplitude (namely, by utilizing an actively balanced interferometer), then one would expect the highest peak at 76 MHz, another high peak at 10 MHz, and the remaining peaks having much smaller amplitudes.

To overcome the phase drift problem, future tests can include an active interferometer balancing system, where a feedback DC bias is used to set the interferometer at its maximum quadratic point.

IV. Ranges and Limitations

The minimum detectable vibration amplitude was on the order of $\Delta_s = 1$ nm. Several factors limited the sensitivity of our sensor. These are 1) low optical power (submicrowatts), where noise in the detection electronics dominate; 2) reduced contrast ratio because of the additional losses suffered due to input/output optics in the sample side and excitation of slab modes in the waveguide; and 3) signal drift due to unbalanced interferometer.

The acoustic spectrum analysis experiments were carried out to frequencies up to 200 MHz at spectral resolution of 600 kHz. For low frequency experiments (kHz range), the spectral resolution was 200 Hz. The sensor was designed to work up to 3–4 GHz. This limitation is due to the bulk design of the modulator electrodes. It is possible to design electrodes to achieve frequencies as high as 100 GHz using traveling wave electrodes [28]. A

TABLE I
MEASUREMENT RANGES (UNKNOWN VALUES MARKED BY DASH)

	Parameter	Current Capability (Measured up to)	Ultimate Measurability
1.	Acoustic Amplitude	1 nm	-
2.	Frequency	0 - 3 GHz (0 - 0.2 GHz)	0 - 100 GHz
3.	Depth Resolution (For $\nu = 5$ km/s)	1.7 μm	50 nm
4.	Longitudinal Resolution Range (Planar)	300 μm - 3 mm	1.3 μm - 1 cm

solid with sound velocity of 5 km/s and modulation speeds up to 100 GHz correspond to a depth resolution (assuming we can only resolve one acoustic wavelength) of 50 nm. The transverse resolution is controlled by the probe beam spot size, which can be as small as one wavelength (1.3 μm) and as large as 1 cm.

The limitations of the technique are summarized in Table I, where the current results and ultimate measurability are presented.

V. CONCLUSION

In this paper, we presented a nonlinear EO polymer-based acoustic spectrum analyzer. Because of the deteriorated response of photodetectors at high frequencies, a heterodyning interferometer is needed to detect vibrations in the GHz frequencies. The sensor presented here is capable of determining the frequency, amplitude, and relative phase of the vibration.

A number of low frequency experiments were conducted to prove the proposed concept. It was possible to detect multiple frequencies and show that the device works as a linear system. It was shown that digital filtering and post processing the sensor data result in a cleaner signal, hence increased detection sensitivity. The device was capable of detecting vibration amplitudes as small as 1 nm.

Finally, the sensor was used to detect pulsed laser excited vibrations at frequencies up to 200 MHz. Because of the bulk electrode geometry, the detection frequency is limited to approximately 3–4 GHz. By making use of traveling wave electrodes, it is possible to achieve modulation frequencies over 100 GHz. Thus, EO polymer-based sensors have the potential to operate at these frequencies.

REFERENCES

[1] S. G. Pierce, W. R. Philp, A. Gachagan, A. McNab, G. Hayward, and B. Culshaw, "Surface-bonded and embedded optical fibers as ultrasonic sensors," *Appl. Opt.*, vol. 35, pp. 5191–5197, 1996.

[2] M. A. Mentzer, "Fiber optic sensors," in *Photonic Devices and Systems*, R. G. Hunsperger, Ed. New York: Marcel Dekker, 1994, pp. 247–277.

[3] D. A. Egan, S. W. James, and R. P. Tatam, "A polarization-based optical fiber vibrometer," *Meas. Sci. Technol.*, vol. 8, pp. 343–347, 1997.

[4] R. G. Hunsperger, *Integrated Optics: Theory and Technology*, 3rd ed. New York: Springer-Verlag, 1996, pp. 305–310.

[5] O. Parriaux, "Integrated optics sensors," in *Advances in Integrated Optics*, S. Martelluci, A. N. Chester, and M. Bertolotti, Eds. New York: Plenum, 1994, pp. 227–242.

[6] M. Tabib-Azar, *Integrated Optics, Microstructures, and Sensors*. Norwell, MA: Kluwer Academic, 1995.

[7] W. B. Jones Jr., *Introduction to Optical Fiber Communication Systems*. New York: Holt, Rinehart and Winston, 1987, pp. 231–232.

[8] G. Tas, R. J. Stoner, H. J. Maris, G. W. Rubloff, G. S. Oehrlein, and J. M. Halbout, "Noninvasive picosecond ultrasonic detection of ultrathin interfacial layers: CF at the Al/Si interface," *Appl. Phys. Lett.*, vol. 61, pp. 1787–1789, 1992.

[9] H. Maris, "Picosecond ultrasonics," *Scientif. Amer.*, pp. 86–89, Jan. 1998.

[10] C. Thomsen, H. T. Grahn, H. J. Maris, and J. Tauc, "Surface generation and detection of phonons by picosecond light pulses," *Phys. Rev. B*, vol. 34, pp. 4129–4138, 1986.

[11] C. J. Morath, G. J. Collins, R. G. Wolf, and R. J. Stoner, "Ultrasonic multilayer metal film metrology," *Solid State Technol.*, pp. 85–92, June 1997.

[12] H.-N. Lin, H. J. Maris, L. B. Freund, K. Y. Lee, H. Luhn, and D. P. Kern, "Study of vibrational modes of gold nanostructures by picosecond ultrasonics," *Appl. Phys. Lett.*, vol. 73, pp. 37–45, 1993.

[13] C. J. Morath and H. J. Maris, "Phonon attenuation in amorphous solids studied by picosecond ultrasonics," *Phys. Rev. B.*, vol. 54, pp. 203–213, 1996.

[14] G. Tas, C. J. Morath, and H. J. Maris, "Reflection of high-frequency acoustic phonons from solid–liquid interfaces studied by picosecond ultrasonics," *Physica B*, pp. 219–220, 660–662, 1996.

[15] H.-N. Lin, R. J. Stoner, and H. J. Maris, "Nondestructive testing of microstructures by picosecond ultrasonics," *J. Nondestructive Eval.*, vol. 9, pp. 239–246, 1990.

[16] Y. H. Berthelot and J. Jarzynski, "Directional laser generation and detection of ultrasound with arrays of optical fibers," *J. Nondestructive Eval.*, vol. 9, pp. 271–277, 1990.

[17] F. A. McDonald, "On the calculation of laser-generated ultrasound pulses," *J. Nondestructive Eval.*, vol. 9, pp. 223–228, 1990.

[18] B. R. Tittmann, R. S. Linebarger, and R. C. Addison Jr., "Laser-based ultrasonics on Gr/epoxy composite," *J. Nondestructive Eval.*, vol. 9, pp. 229–238, 1990.

[19] J.-P. Monchalin and J.-D. Aussel, "Ultrasonic velocity and attenuation determination by laser-ultrasonics," *J. Nondestructive Evaluation*, vol. 9, pp. 211–221, 1990.

[20] Y. Lin, M. Sansalone, and N. J. Carino, "Finite element studies of the impact-echo response of plates containing thin layers and voids," *J. Nondestructive Eval.*, vol. 9, pp. 27–47, 1990.

[21] H. T. Grahn, D. A. Young, H. J. Maris, J. Tauc, J. M. Hong, and T. P. Smith III, "Sound velocity and index of refraction of AIA's measured by picosecond ultrasonics," *Appl. Phys. Lett.*, vol. 53, pp. 2023–2024, 1988.

[22] R. J. D. Miller, R. Casalegno, K. A. Nelson, and M. D. Fayer, "Laser-induced ultrasonics: A dynamic holographic approach to the measurement of weak absorptions, optoelastic constants and acoustic attenuation," *Chem. Phys.*, vol. 72, pp. 371–379, 1982.

[23] A. Yacoubian, V. Chuyanov, S. M. Garner, H. Zhang, W. H. Steier, A. S. Ren, G. Todorova, and L. R. Dalton, "Acoustic spectrum analysis using polymer integrated optics," in *Proc. OSA/ACS Organic Thin Films*, Sept. 1999.

[24] S. Kalluri, M. Ziari, A. Chen, V. Chuyanov, W. H. Steier, D. Chen, B. Jalali, H. Fetterman, and L. R. Dalton, "Monolithic integration of waveguide polymer electrooptic modulators of VLSI circuitry," *IEEE Photonics Technol. Lett.*, vol. 8, pp. 644–646, 1996.

[25] C. Gorecki, "Sub-micrometric displacement measurements by an all-fiber laser heterodyne interferometer using digital phase demodulation," *J. Opt.*, vol. 26, pp. 29–34, 1995.

[26] F. Tian, R. Ricken, and W. Sohler, "High performance integrated acousto-optical heterodyne interferometer in $LiNbO_3$," in *Proc. Optical Fiber Sensors Conf. '93*, Florence, Italy, 1993, pp. 263–266.

[27] F. Tian, R. Ricken, St. Schmid, and W. Sohler, "Integrated acousto-optical heterodyne interferometers in $LiNbO_3$," in *Proc. LASER '93*, Munich, Germany, 1993, pp. 725–728.

[28] D. Chen, H. R. Fetterman, B. Tsap, A. Chen, and W. H. Steier, "Next generation ultra-high frequency integrated EO modulators," in *OSA Tech. Dig. Series*, vol. 14, 1997, pp. 224–225.

[29] Y. Shi, C. Zhang, H. Zhang, J. H. Bechtel, L. R. Dalton, B. H. Robinson, and W. H. Steier, "Low (sub-1-volt) halfwave voltage polymeric electro-optic modulators achieved by controlling chromophore shape," *Science*, vol. 288, pp. 119–122, 2000.

[30] R. M. Gagliardi and S. Karp, *Optical Communications*, 2nd ed. New York: John Wiley and Sons, 1995.

[31] R. W. Boyd, *Radiometry and the Detection of Optical Radiation*. New York: Wiley, 1983.

[32] A. U. Rehman, C. Potel, and J. F. de Belleval, "Modeling of ultrasonic beam interaction with an anisotropic multilayered medium, using angular spectrum method," in *Acoustical Imaging*, S. Lees and L. A. Ferrari, Eds. New York: Plenum, 1997, vol. 23, pp. 399–404.
[33] F. Wang, A. S. Ren, M. He, A. W. Harper, L. R. Dalton, S. M. Garner, A. Chen, and W. H. Steier, "High electro-optic coefficient from a polymer containing high $\mu\beta$ chromophores," Polymer Mater. Sci. Eng., vol. 78, to be published.
[34] A. Yacoubian, W. Lin, D. Olson, and J. Bechtel, "Compact EO polymer vibration sensor utilizing ridge and slab-mode waveguides," in *ACS Proc. Organic Thin Films for Photonic Applications*, Washington, DC, Mar. 2000.
[35] R. A. Guyer and P. A. Johnson, "Nonlinear mesoscopic elasticity: Evidence for a new class of materials," *Phys. Today*, pp. 30–36, Apr. 1999.

Araz Yacoubian received the B.S. degree in optical engineering from the University of La Verne in 1989, and the M.S. in electrical engineering-systems and the Ph. D. in electrical engineering-electrophysics from the University of Southern California, Los Angeles, in 1993 and 1999, respectively.

He was a Research Engineer with the Physical Optics Corporation (POC) between 1989 and 1991, and later worked as a Consultant, where he conducted research on holography, holographic and nonlinear optical materials, and holographic optical elements. From 1993 to 1995, he was with the Jet Propulsion Laboratory, Pasadena, CA, as a mMember of Technical Staff, academic part-time, were he worked on optical image processing, automatic target recognition, wavelet-based feature extraction, and developing a deployable image processing system. He joined Integrated Photonic Technology (IPITEK), Carlsbad, CA, in January 2000 as a Staff Scientist in charge of the optical polymer device program. He has been active in developing high speed polymer modulators and sensors.

Vadim Chuyanov, photograph and biography not available at the time of publication.

Sean M. Garner, photograph and biography not available at the time of publication.

William H. Steier, photograph and biography not available at the time of publication.

Albert S. Ren, photograph and biography not available at the time of publication.

Larry R. Dalton, photograph and biography not available at the time of publication.